Moisture Effect on the Threshold Switching of TOPO-Stabilized sub-10 nm HfO_2 Nanocrystals in Nanoscale Devices

*Sonam Maiti[1,§], Thorsten Ohlerth[2,§], Niclas Schmidt[1,3], Stephan Aussen[1,3], Rainer Waser[1,4], Ulrich Simon[2], Silvia Karthäuser[1]**

[1]Peter Grünberg Institut (PGI-7) and JARA-FIT, Forschungszentrum Jülich GmbH, Jülich 52425, Germany.

*E-Mail: s.karthaeuser@fz-juelich.de

[2] Institute of Inorganic Chemistry and JARA-FIT, RWTH Aachen University, Aachen 52074, Germany

[3]RWTH Aachen University, Aachen 52062, Germany

[4]Institute of Materials in Electrical Engineering and Information Technology II and JARA-FIT, RWTH Aachen University, 52074 Aachen, Germany

§ These authors contributed equally to this work.

Abstract

The enduring demand for ever increasing storage capacities inspires the development of new few nanometer-sized, high-performance memory devices. In this work, tri-*n*-octylphosphine oxide (TOPO)-stabilized sub-10 nm monoclinic HfO_2 nanocrystals (NC) with rodlike and spherical shape are synthesized and used to build-up microscale and nanoscale test-devices. The electrical characterization of these devices studied by cyclic current-voltage measurements reveals a redox-like behaviour in ambient atmosphere and volatile threshold switching in vacuum. Employing a thorough spectroscopic and surface analysis (FT-IR, NMR, XPS) the origin for this behaviour was elucidated. While the redox-behaviour is enabled by residual moisture present during clean-up of the NC and thin film preparation, which leads to a partial desorption of TOPO from the NC surface, threshold switching is obtained for dry TOPO-stabilized HfO_2 NC in microchannel as well as in nanoelectrode devices addressing only a few sub-10 nm TOPO-stabilized HfO_2 NC. The results show that integration of sub-10 nm HfO_2 NC in nanoscale devices is feasible to build up switching elements.

1. Introduction

The enduring aspiration to minimize electronic devices driven by the high request for non-volatile data storage as well as the demand for printed electronics on flexible supports promotes the application of ultrathin films or nanocrystals (NC) in future memory devices.[1-3] Consequently tracing this goal, that is, downscaling of the switching layer thickness as well as the effective electrode area, the addressing of an individual NC between two nanosized electrodes becomes the reasoned, technically feasible next step, like we have shown recently.[4-8] As today's state-of-the-art hafnium oxide (HfO_2) exhibits qualitative advantages for a variety of applications in nanoelectronics and outperforms traditional oxide materials as it holds an outstanding chemical stability, high melting point, high dielectric constant, wide bandgap, and transparency in the region from infrared to ultraviolet.[1] HfO_2 is used in metal–oxide semiconductor field-effect transistors, ferroelectric field-effect transistors, highly-scaled dynamic random access memories, and resistive random access memories (ReRAM). Especially, its proven CMOS compatibility and full scalability makes it an advantageous material for future nanoelectronic devices.[1,9-11] It is known that in HfO_2 ReRAM the resistive hysteresis is generated by an oxygen vacancy drift and linked redox reactions due to an applied electric field.[9,12,13]

A well-established ligand for the synthesis of NC is tri-*n*-octylphosphine oxide (TOPO), which enables the formation of nanocrystallites with narrow size distribution and a high colloidal stability in organic solvents. TOPO itself is soluble in a variety of common solvents, such as toluene, hexane, or methanol. While its popularity as capping ligand stems from the intense studies on predominantly CdSe NC, based on its low cost it is meanwhile widely applied to a plethora of nanoparticle classes.[14] A capping ligand for HfO_2 NC needs to meet another important physical feature beyond its chemical ones. Since it will fill the space between the NC, it should exhibit a higher resistivity than HfO_2 to ensure that it does not form a preferred conducting path in HfO_2 NC devices. As will be shown later this condition is fulfilled for TOPO in TOPO-HfO_2 NC thin films. Due to its advantageous properties, we also employ here TOPO

as capping ligand for the synthesis of HfO_2 NC, which are hence designed for the use in electronic devices. In that manner, we take special care about the environmental conditions during synthesis, device fabrication and characterization of the electronic properties in test devices of TOPO-HfO_2 NC.

A very recent study on HfO_2 NC multilayers reported resistive switching properties to correlate with the length of the molecules forming the organic capping layer.[15] This finding leads to the important question, to which extend the ligand properties can affect the electronic properties of a semiconductor NC? This question will be particularly relevant, when the NC will be integrated into devices, as changed interface properties will have a significant effect on the device functionality, performance, and stability, as well. These two aspects, i. e. the effect of the TOPO binding motive on the properties of the individual NC as well as on the device functionality, will be addressed in this study by probing TOPO-stabilized monoclinic HfO_2 NC with two different morphologies, i. e. rodlike and spherical shaped particles that differ in surface termination.

2. Experimental Section

2.1. Synthesis of HfO_2 Nanocrystals

The synthesis of rodlike HfO_2 NC was adopted from Tang et al.[16] and modified as described in the following to receive monoclinic phase particles with nearly spherical shape. Acetone (≥ 99.8%, VWR) and toluene (≥99.5%, VWR) were used as received. The precursors hafnium(IV)chloride (99.9%, ABCR), hafnium(IV)isopropoxide (99%, Alfa Aesar) and hafnium(IV) 2,4-pentanedionate (97% Alfa Aesar) were used without further purification. TOPO (98%, Alfa Aesar) was degassed and flushed with argon several times at 120 °C and ~$1x10^{-3}$ mbar for one hour prior to use. All syntheses were performed under inert gas atmosphere. For the synthesis of the rod-shaped monoclinic phase particles, equimolar amounts of $HfCl_4$ (2 mmol, 0.64 g) and Hf(isopropoxide)$_4$ (2 mmol, 0.95 g) were added to 10 g

of melted TOPO (~60 °C). The reaction mixture was stirred vigorously and heated up to 340 °C, kept at that temperature for 2 hours and was afterwards cooled down to 80 °C. At that point, acetone was added to the reaction mixture so that excess TOPO could be removed, and the surface functionalized particles were collected as precipitate. The rod-shaped particles were purified through several redispersion (in acetone) and centrifugation steps. The reaction protocol for the newly introduced monoclinic HfO_2 NC with spherical shape was analogue to the above mentioned with the difference that the precursor mixture was exchanged towards equimolar amounts of $HfCl_4$ (2 mmol, 0.64 g) and $Hf(acac)_4$ (2 mmol, 1.15 g) instead. A colloidal suspension of HfO_2 NC could be readily stabilized for several days through redispersing the precipitate in toluene via ultrasonification. Redispersion was conducted in two ways: under ambient conditions in as-received toluene resulting in TOPO-HfO_2 NC with residual moisture (NC(rm)), and via three repetitional steps involving dispersing NCs in sodium dried toluene and high vacuum pump cycles yielding water free TOPO-HfO_2 NC (NC(dry)).

2.2. Microchannel and Nanoelectrode Structures

As microchannel structures, commercially available OFET structures on silicon (Fraunhofer IPMS, Germany) were used. They are formed by Au source and drain electrodes (30 nm) patterned on a SiO_2 gate-insulator (230 nm) covering n-doped silicon (size of wafer pieces = 15 mm x 15 mm). For electrical measurements we used the interdigitated electrode structures with channels of 2.5 µm or 5 µm width and 10 mm length (Supporting Information, Figure S1).

The nanoelectrode devices were fabricated on 25.4 mm x 25.4 mm wafer pieces covered with 400 nm SiO_2 using electron beam lithography technique (Raith EBPG 5200, 100 keV). A lift-off process was applied using the high-resolution e-beam resist (CSAR 6200.04, ALLRESIST GmbH) with a resist layer thickness of 100 nm. After writing of the nanoelectrode structures development was performed in AR 600-55 (ALLRESIST GmbH) for 1 min. Physical vapor deposition was used for metallization (1 nm Ti, 20 nm Au) and lift-off was conducted in acetone

overnight. After processing, the wafer pieces were cut into 6 mm x 6 mm fractions resulting in nine individual samples with 12 nanoelectrode pairs each, exhibiting a 20 ± 1.5 nm gap in between. Beside microchannel devices these nanogap devices were employed to fabricate HfO_2 NC test devices, too (Supporting Information, Figure S1).

2.3. Thin-Film Preparation

Well-ordered films of TOPO capped HfO_2 NC were assembled by using an evaporation-based deposition method (Supporting Information, Figure S2). To ensure that reliable results concerning the performance of the NC films are received, a stock solution of each nanoparticle class of HfO_2 NC was diluted with toluene (used as received (≥99.5%, VWR) or dried with molecular sieves resulting in a H_2O content of 30 ppm, respectively) and checked with SEM for assembling consistency (~1-2 mg of dry HfO_2 NC in 10 ml of dry toluene). The employed electrode structures on wafer pieces were cleaned prior to use in an ultrasonic bath for 10 min in acetone, 10 min in isopropanol, and then blown dry with N_2, while the used 200 nm Au thin films on mica were rinsed with isopropanol and then blown dry.[17] The self-assembled HfO_2 NC thin films for electrical characterization were deposited under different atmospheric conditions, i. e. in an ambient environment and in an argon filled glovebox (H_2O < 10 ppm). 40 µl and 20 µl HfO_2 NC solution were used to assemble NC into the gap between the electrodes in micrometer and nanometer scale devices, respectively (Supporting Information, Figure S3). The films dried within almost 2 hours while the evaporation rate of toluene was controlled (Supporting Information, Figure S2). TOPO thin films were prepared accordingly. In this case, 40 µl and 20 µl of a TOPO solution in dry toluene (1 mg/ml) were dropped onto the microchannel and nanogap devices, respectively. The same procedure was applied for preparing XPS samples on gold substrates. Here 30 µl of the HfO_2 NC solution were used under different atmospheric conditions.

As reference for the XPS measurements, HfO_2 films were deposited by atomic layer deposition (ALD). 30 nm HfO_2 were grown from tetrakis(ethymethylamido)hafnium and oxygen plasma as co-reactant at 300°C. Process details can be found in reference.[18]

2.4. Instrumentation

2.4.1. ***Nanoparticle characterization*.** Particle size, shape and crystal phase were determined with standard bright field imaging techniques and selected area electron diffraction analysis (SAED) by transmission electron microscopy (TEM) on a ZEISS LIBRA 200 FE microscope operating at 200 kV. The HfO_2 NC dispersed in toluene were drop-casted onto a carbon coated copper grid (200 mesh, 3-4 nm, Science Services) for characterization. Scanning electron microscopy (SEM) was conducted with a high-resolution field emission SEM (LEO/ZEISS Supra 35 VP, Germany). Fourier transform infrared (FT-IR) spectra were acquired from pellets containing ~180 mg dry KBr and 2-4 mg of the respective compound with a Vertex 70 FT-IR spectrometer (Bruker Optics). Nuclear magnetic resonance (NMR) experiments were recorded with a Bruker Avance-II-400 MHz Instrument (Bruker). Chemical shifts were referenced against tetramethylsilane (TMS) referring to remnant proton signals that stem from deuterated chloroform ($CDCl_3$). HfO_2-NCs or TOPO with residual water were dispersed under ambient conditions in $CDCl_3$, whereas dried samples were dispersed within an argon filled glovebox in $CDCl_3$ that was prior distilled over calciumhydride.

2.4.2. ***Device characterization*.** Electrical measurements were performed under ambient and vacuum conditions (10^{-6} mbar) at room temperature in a probe station equipped with tungsten probes. The cyclic current versus voltage (*I*/*U*) characteristics were recorded using a subfemtoamp remote source meter unit (Keithley 6430). SEM images of the device structures were taken after completion of all transport measurements.

2.4.3. ***X-Ray photoelectron spectroscopy (XPS)*.** XPS was conducted with a Phi5000 VersaProbe II (ULVAC-Phi Inc., USA) provided with monochromatic Al Kα radiation (1.486 keV). Survey scans (187.5 eV pass energy, 0.8 eV step) and core level spectra (23.5 eV, 0.1

eV step) of Hf 4f, O 1s, C 1s, P 2p were recorded. The binding energies were corrected for electrical charge effects by referencing to the C 1s peak, which was set to 285 eV. Data fitting was performed using Gauss–Lorentz profiles and a Shirley-background was used.

3. Results and Discussion

3.1. HfO_2 Nanocrystal Characterization

HfO_2 NC capped with TOPO were synthesized with two different shapes, nanorods and spheres (Figure 1), following previously published[16] and the described above, modified procedures, respectively. While spherical shaped HfO_2-NCs were also synthesized via this sol-gel method, their crystal phase displayed the tetragonal phase. We deliberately aimed to synthesize isotropic particles in the monoclinic crystal phase in order to vary only between the morphology of the NCs. When $Hf(acac)_4$ is used instead of $Hf(isopropoxide)_4$ during the synthesis, the obtained NCs could be stabilized in the monoclinic phase like the rodlike NCs (see Figure S4 for SAED analysis).

Transmission electron microscopy (TEM) images (Figures 1) reveal rodlike NCs with a length of 8.2 nm and a width of 2.0 nm, while the mean diameter of the spherical NC is (5.8 ± 0.9) nm, based on counting at least 200 NC per sample. The TEM images further indicate that the here called spherical NCs are facetted crystals, yet the crystal surfaces are not developed in a fashion that allows for exact face determination. Since the aspect ratio of these NCs is close to unity and for simplicity reasons, they are called here spherical HfO_2 nanocrystals. The scanning electron microscope (SEM) image of the self-assembled, rodlike TOPO-HfO_2 NC thin film (Figure 1c) indicates a highly ordered monolayer with an average particle spacing of (2.12 ± 0.5) nm. This is slightly less than twice the length of TOPO molecules (2 × 1.18 nm = 2.36 nm) and thus, indicates coiling and/or interdigitation of the protruding alkyl chains to some extent. Interdigitation is promoted by van der Waals interactions between the octyl chains of TOPO ligands on neighbouring HfO_2 NC, like also observed in TOPO crystals,[19,20] and enables

a high degree of order in the self-assembled NC film fabricated at low evaporation rates of the solvent.

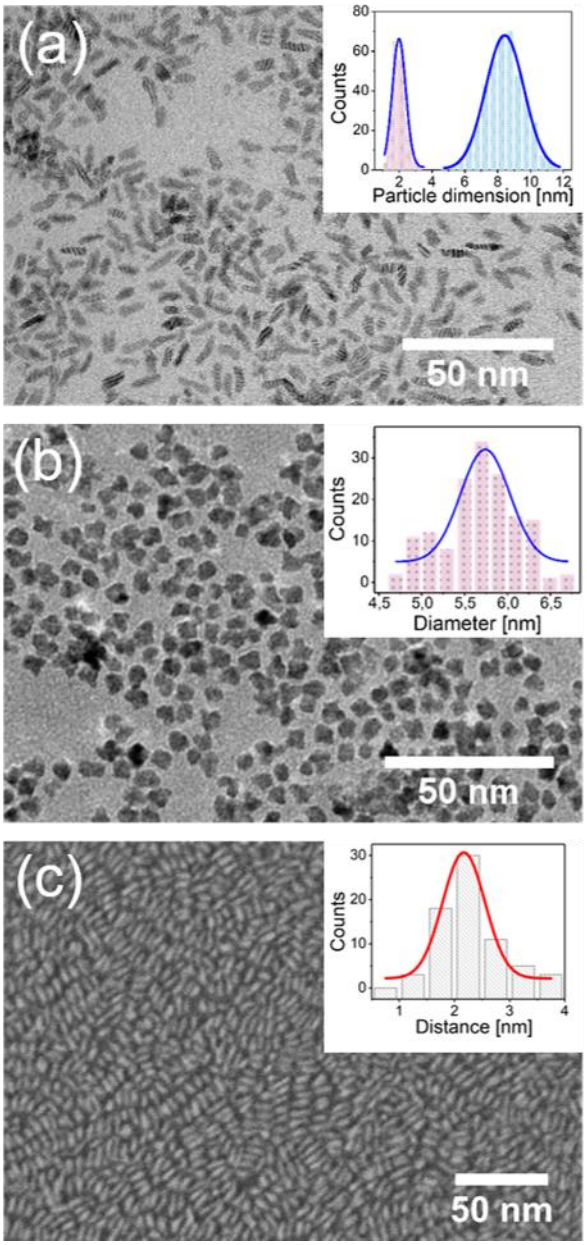

Figure 1. TOPO-HfO_2 NC. (a) TEM image of rodlike NC (inset: size distribution). (b) TEM image of spherical NC (inset: size distribution) (c) SEM image of a self-assembled film of rodlike NC (inset: distribution of the spacing between NC).

The TOPO-HfO_2 NC were further characterized by FT-IR and ^{31}P as well as ^{1}H NMR spectra. By comparing the FT-IR spectra of the TOPO capped nanocrystals with that of the free ligand

molecules (Figure 2), the adsorption of TOPO on the HfO_2 NC surface was verified. While the ν_{OH} (residual water) at 3420 cm^{-1} and the ν_{CH2} stretching modes at 2924 cm^{-1} and 2850 cm^{-1} remain unchanged, the $\nu_{P=O}$ stretching absorption band is red-shifted for the TOPO-HfO_2 NC to 1109 cm^{-1}, compared to the band at 1145 cm^{-1} characteristic for TOPO, and simultaneously broadened.[20,21] This broadening, denoting less defined P=O species in TOPO-HfO_2 NC, is likely caused by the bonding of the P=O group to the NC surface exhibiting different facets. It is a clear indication that the P=O group is chemically altered by the nanoparticle surface.

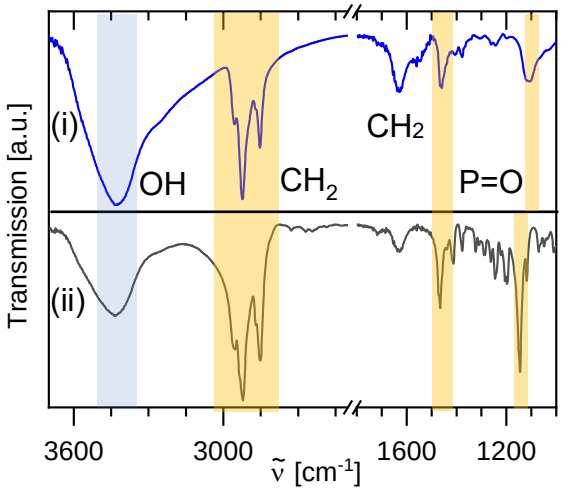

Figure 2. FT-IR spectra. (i) Rodlike TOPO-HfO_2 NC, (ii) TOPO molecules.

^{31}P NMR and ^{1}H NMR analysis, that are very sensitive to changes in chemical bonds, reveal further insights into the TOPO coordination at the HfO_2 NC surface (Figure 3). While a ^{31}P NMR signal at 48.9 ppm is characteristic for pure TOPO in dry solvent (TOPO(dry)), this signal shifts slightly to 50.5 ppm if residual water or H-bonds are present (TOPO(rm)).[22,23] Interestingly, this TOPO signal vanishes completely in case of dried TOPO-HfO_2 NC (hereafter abbreviated as NC(dry)) and only one signal at 74.5 ppm is resolved which we attribute to hafnia bound TOPO. More specifically, this signal is identified as a hydroxytri-*n*-octylphosphonium cation species in literature and these species are believed to bind to the NC surface of colloidal hafnia.[24] It should be emphasized in this context, that the signal is not concordant with hypothetical by-products like octyl dioctylphosphinate (57.8 ppm), dioctyl

octylphosphonate (32.8 ppm), dioctylphosphinic acid (60.4 ppm) or octylphosphonic acid (37.7 ppm).[23] However, in the sample of the identical TOPO-HfO_2 NC but with residual moisture (hereafter abbreviated as NC(rm)), that originates from the clean-up process under ambient conditions with as received toluene, the intensity of the signal at 74.5 ppm is reduced and the ^{31}P TOPO signal at 48.9 ppm appears, pointing at a partial desorption of TOPO molecules from the NC.

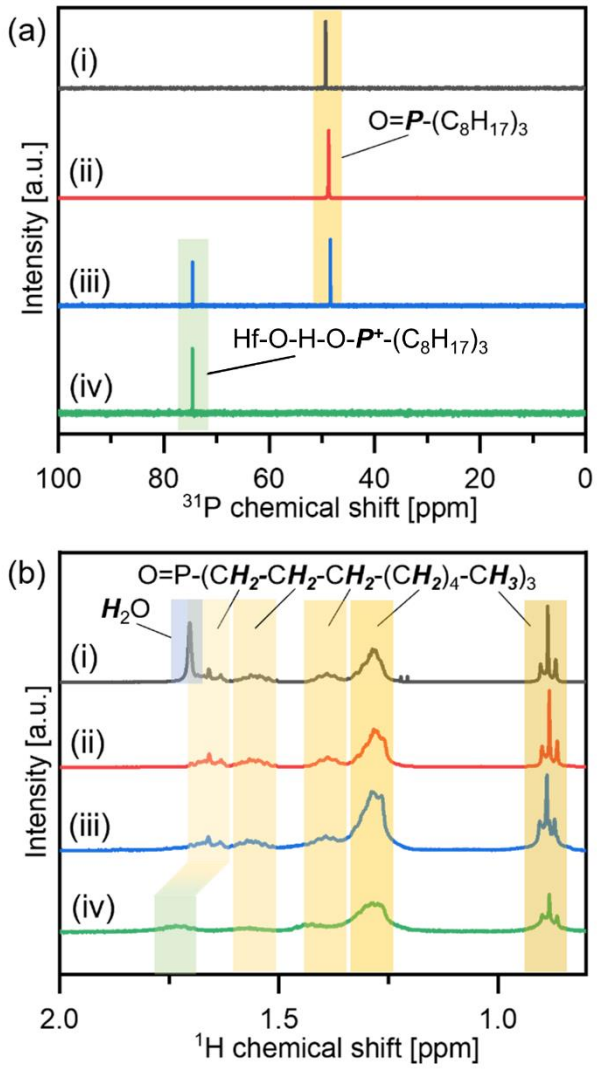

Figure 3. NMR spectra. (a) ^{31}P NMR and (b) ^{1}H NMR of (i) TOPO in toluene as received, (ii) TOPO in dry toluene, (iii) NC(rm), (iv) NC(dry).

Accordingly, the ^{1}H NMR spectra exhibit a similar trend for all samples and the NC(dry) are generally lower in signal intensity. The phosphorus adjacent alky-CH_2 chain units are observed

at 1.64-1.73 ppm for free TOPO, that is, in samples (i)-(iii). Especially the dominance of free TOPO in case of NC(rm) verifies its desorption from the NC surface in the presence of moisture. On the other hand, the corresponding CH_2 chain units in the Hf-O-H-O-P^+R_3 species (1.71-1.79 ppm) exist in dry conditions only, i.e. in sample NC(dry). This phosphorus adjacent CH_2-chain unit is influenced by the electron density of the P=O headgroup. Since it is surrounded by less electron density in the Hf-O-H-O-P^+R_3 arrangement, it is more strongly affected by the magnetic field. As a consequence, we observe a deshielding effect. Similar observations for a signal shift for this specific CH_2 unit have been made in the same solvent ($CDCl_3$) by another group, for TOPO and TOPO-H_2O_2 adducts.[19] In this way, FT-IR and NMR spectroscopy confirm not only the adsorption of TOPO at the HfO_2 NC surface but point also to the possibility of TOPO desorption in the presence of traces of water.

For a further elucidation of the effect of residual moisture on TOPO stabilized HfO_2 NC and a possible impact on the performance of TOPO-HfO_2 NC devices more information about the surface chemistry of the NC is required. Therefore, the dependence of the surface composition and the oxidation states of the TOPO-HfO_2 NC on the absence or presence of small amounts of residual water during the clean-up or film preparation steps was analyzed by XPS. The results obtained from Hf 4f and O 1s core level spectra are given in Figure 4 and summarized in Table1. The two hafnia peaks Hf $4f_{5/2}$ and Hf $4f_{7/2}$ are fitted with a doublet with fixed intensity ratio 3:4 and a separation of 1.71 eV. Here we discuss the main peak Hf $4f_{7/2}$ at lower binding energy (BE). In Figure 4 (i) and (ii) two reference spectra are given characterizing a dry 30 nm HfO_2 layer fabricated by ALD and a TOPO(rm) film deposited on such a layer, respectively. While the dry ALD film shows exclusively the expected Hf^{IV} peak at 16.9 eV, the spectrum of TOPO(rm) presents also a new peak at a BE of 18.2 eV which we attribute to the formation of hafnium hydroxide caused by the presence of moisture.[25] In contrary, the Hf 4f spectrum from dry NC (iv) is characterized by a single peak at 17.4 eV, which corresponds to the HfO_2 peak shifted to a higher BE due to the TOPO capping layer. The H 4f spectrum from spherical NC(rm) films (iii) exhibits two peaks, one characteristic for Hf^{IV} at a BE of 17.1 eV and one lower intensity peak at BE = 17.8 eV. Even though the latter peak is in the range for hafnia

hydroxide, its value points to possible contributions of Hf-O-H-O-P^+R_3 species, thus indicating a partial desorption of TOPO (for Hf 4f core level spectra of rodlike TOPO-HfO_2 NC see Supporting Information, Figure S5).

The O1s spectra can be decomposed into up to three components. The peaks centered at 530.1 eV correspond to oxidic species (O^{-II}), at 531.8 eV to hydroxide species (OH^-), and water appears at 533.2 eV, respectively.[25,26] A possible C=O peak (BE in the range 532.0 eV to 532.4 eV) is usually found in the same energy range as the hydroxides.[26,28] In the O 1s spectra (ii) and (iii), associated to TOPO(rm) and NC(rm), we find as expected a peak at 531.7-531.8 eV indicating hydroxide, which is related to the Hf 4f peaks at around 18.0 eV and verifies the above assignment. For the multilayer of TOPO(rm) even a small contribution revealing water is detected. It should be noted that the observed O 1s peak with lower intensity at 531.8 eV, visible in the spectrum of the HfO_2 ALD film (i), is attributed to carbonyl oxygen ($R_2C=O$) or carbon monoxide (C=O) since there is no counterpart in the Hf 4f spectrum. In addition, small amounts of carboxylates may be present as well, as indicated by the corresponding C 1s core level spectrum given in Figure S6. These small amounts of carbonyl or carboxyl compounds are possible byproducts of the plasma-enhanced ALD process at 300°C while carbon monoxide might be a result of surface contamination due to the ambient transfer from the ALD system to the XPS system.[27]

The O 1s spectrum for NC(dry) (iv) again differs from the core-level spectra from species containing residual moisture. Here we find O 1s peaks at 530.7 eV and 532.2 eV distinctly shifted to higher BE. While we attribute the peak at 530.7 eV to surface HfO_2 indirectly influenced by TOPO, the BE 532.2 eV corresponds to Hf-O-H-O-P^+R_3 with R = octyl. The P 2p core level spectra give additional verification to the assignment of the Hf 4f and O 1s peaks. While for NC(rm) also a P $2p_{3/2}$ peak at 132.8 eV is obtained, corresponding to free TOPO molecules, a value of 133.3 eV is recorded for NC(dry) denoting bound TOPO (Supporting Information, Figure S7).[29]

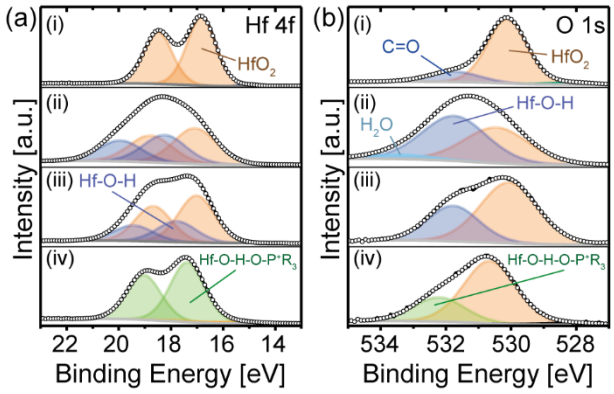

Figure 4. XPS spectra (a) Hf 4f core level spectra, (b) O1s core level spectra of (i) dry HfO_2 ALD film (reference), (ii) dry HfO_2 ALD film + TOPO(rm) film, (iii) spherical NC(rm), (iv) spherical NC(dry).

Table 1. XPS binding energies (eV) for HfO_2 ALD films and spherical TOPO-HfO_2 NC.

Material	**Hf 4f$_{7/2}$**			**O 1s**			
	HfO_2	**Hf**-O-H-O-P^+R_3	**Hf**$O(OH)_2$	Hf**O**$_2$	Hf$O($**O**$H)_2$/ C=**O**	Hf-O-H-**O**-P^+R_3	H_2**O**
ALD film	16.9			530.1	531.8		
ALD film + TOPO(rm)	17.1		18.2	530.4	531.7		533.4
NC(rm)	17.0		17.8	530.1	531.8		
NC(dry)		17.4		530.7		532.2	

These data confirm that our procedure to exclude consequently moisture in the TOPO-HfO_2 NC clean-up or thin film preparation is effective and leads to pure TOPO-stabilized NC(dry). However, in consistency with FT-IR, NMR, and XPS, we conclude that already very small amounts of introduced moisture lead to a fractional desorption of TOPO. This can be explained via a simple acid-base reaction, where the strong acidic and surface bound H-O-P^+R_3 species (pK_a = -1.5) protonates water molecules,[30,31] while in a second step, the bare oxygen surface sites are basic and prone to be hydroxylized by water again:

$HfO(OHOP^+R_3) + H_2O \rightarrow HfO_2 + O{=}PR_3 + H_3O^+$

$HfO_2 + H_2O \rightarrow HfO(OH)^+ + OH^-$

Which leads to the sum reaction (given traces of water are available):

$HfO(OHOP^+R_3) \rightarrow HfO(OH)^+ + O{=}PR_3$

We assume that the desorption of TOPO molecules from the NC surface basically results from water that is been taken up at the polar bonds between ligand and particle surface. A simplified view of this process is given in Figure 5.

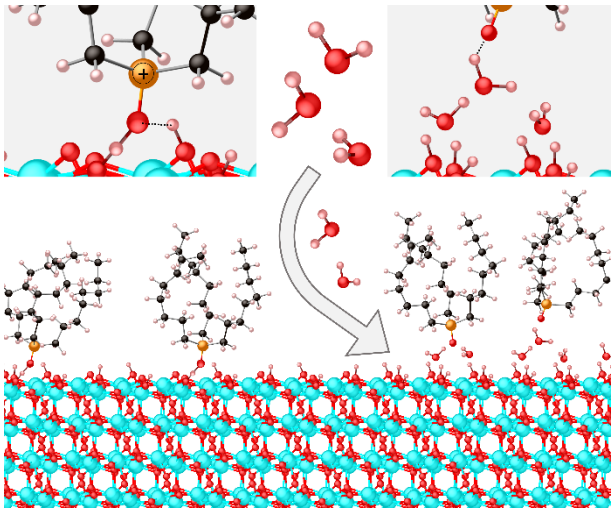

Figure 5. Schematic views of the TOPO-stabilized HfO_2 NC surface under the influence of water. Atoms are displayed with covalent radii while hydrogen is depicted in pink, carbon in black, oxygen in red, phosphorus in gold and hafnium in cyan.

3.2. Electrical Characterization of TOPO-HfO_2 NC films

A first electrical characterization of the monoclinic rodlike and spherical NC(rm) films was performed by cyclic current/voltage (*I*/*U*) measurements using microchannel devices with channel width of 2.5 µm, 5 µm, and 10 µm. Approximately one hundred functional devices have been tested measuring a few to more than 30 *I*/*U*-cycles using varying sweep rates (0.1 mV/sec to 100 mV/sec), and voltage ranges (±1 V to ±10 V). A representative example for the *I*/*U* characteristic of these NC(rm) films, here spherical ones, obtained in ambient atmosphere

with a constant sweep rate of 1 mV/sec in the voltage range ±5 V is given in Figure 6 (for rodlike NC(rm) see Supporting Information, Figure S8). Stable well-defined *I*/*U*-cycles indicating an electrical robustness of the devices were obtained without a dependence on the shape of the TOPO-HfO_2 NC. Comparable cyclic voltammetry curves were measured for all devices tested under ambient conditions with the peak position dependent on the sweep rate only (Supporting Information, Figure S9).

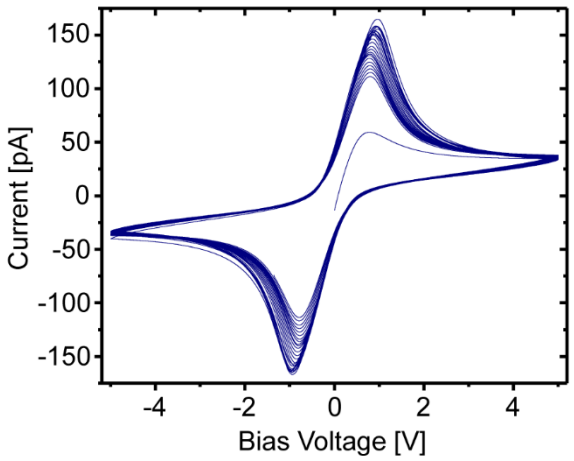

Figure 6. *I*/*U* diagrams of spherical TOPO-HfO_2 NC films (channel width 2.5 µm, ambient atmosphere, and sweep rate 1 mV/sec).

The shape and peak positions of these *I*/*U*-characteristics as well as their independence on the NC(rm) properties strongly suggest a redox-like behavior, like usually found in cyclic voltammograms of water. The standard electrode potential for the oxidation of water is 1.23 V and for the reduction -0.83 V, that is a separation of about 2 V like observed here. Therefore, we designed experiments to determine unambiguously the origin of the redox peaks measured under ambient.

We decided to examine the organic ligand, TOPO, under the influence of moisture in more detail. First, films of TOPO molecules, prior dissolved in as-received toluene for sample preparation in ambient (denoted as TOPO(rm)), were electrically characterized in microchannel devices under atmospheric humidity. Like shown in Figure 7a, they exhibit well-defined cyclic voltammograms with peaks at ±1 V. However, if the TOPO films were prepared

from dry toluene in argon atmosphere (denoted as TOPO(dry)) a distinctly lower current and inconspicuous redox peaks at a considerably higher voltage (±2 V) were received even though the measurement was conducted in ambient (Figure 7b). This points to a major effect of water molecules introduced during the clean-up of NC and thin film preparation on the electric properties of the devices.

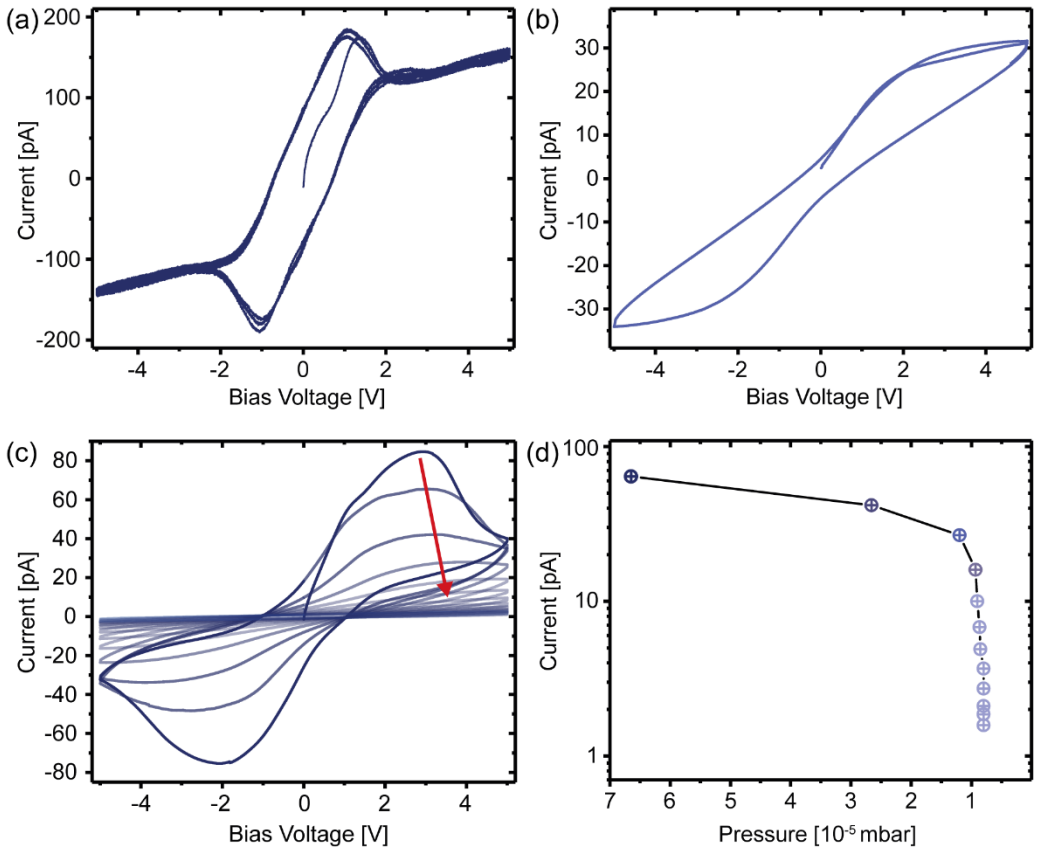

Figure 7. Cyclic voltammetry curves of TOPO films obtained from microchannel arrays with a gap size of 2.5 µm (sweep rate 1 mV/sec). (a) TOPO(rm), (b) TOPO(dry), (c) TOPO(rm) measured under steadily reduced pressure. The red arrow indicates the course of the curves during continuously decreasing pressure (d) Current vs. pressure profile corresponding to the *I*/*U*-cycles given in (c).

Next, a TOPO(rm) sample was examined in a cryostat, while the pressure was continuously reduced by means of a vacuum pump. The strongly pressure dependent reduction of the

current and the considerable shift of the redox peaks towards higher voltages verifies the hypothesis that water plays a significant role in the conduction process (Figure 7c). At the very beginning of the pumping, a very fast decrease of the absolute current value is observed so that no stable cycles could be obtained. Then the drying process slowed down and after reaching the achievable low pressure ($8 \cdot 10^{-6}$ mbar) a further decrease of the device current was observed with time (Figure 7d). We assume, that first water molecules loosely coordinated to TOPO, which form the main contribution to the current, were desorbed, while during ongoing reduction of the pressure a desorption of water molecules directly coordinated to TOPO takes place. The possibility of drying TOPO under vacuum at RT is also reported in literature.[32] Thus, it could be verified that the so far discerned redox peaks observed during the *I*/*U* cycling of NC(rm) films (Figure 6) mainly originate from residual water introduced during clean-up and film preparation. Furthermore, the achievable current in TOPO(rm) films is in the same range as for NC(rm) films, which suggests that the conducting medium in the NC(rm) films is built by TOPO molecules separating the NC which are loaded with water molecules from residual moisture.

Following, in order to prevent this water effect in TOPO-HfO_2 NC films, the clean-up and the thin film preparation were performed in controlled inert atmospheres employing dry toluene. The resulting *I*/*U* curves for these dry NC(dry) film devices measured in vacuum (Figure 8) exhibit a distinctly reduced current, no redox peaks, and the shape is quite different compared to NC(rm) devices affected by residual water molecules. A unipolar hysteretic *I*/*U* characteristic is obtained without any forming step. Starting at 0 V we find the microchannel device initially in the HRS (high-resistive state) and a considerably increasing current is observed starting at about 2 V. Further increasing the voltage results in a self-limiting current, that is, a maximal current which is not limited by a current compliance of the set-up. When the voltage is reduced, the microchannel device takes a hysteretic course and shows a LRS (low-resistance state). If the applied voltage falls below the hold voltage, at about U_{hold} = 1 V, the device turns into its HRS again. In the voltage range, +1 V to -1 V, around Fermi level a near-Ohmic behaviour is observed. With further decreasing voltage, we find the same hysteresis as described for

positive applied voltages. This symmetry can be attributed to the symmetric device design Au/TOPO-HfO_2 NC/Au.[13] It results from in average identical interface interactions at both TOPO-HfO_2 NC/Au interfaces, like described for example for a recently reported Pt/TiO_2/Pt nanobelt device.[33] The *I*/*U* characteristic given in Figure 8a represents volatile threshold switching which has been observed in rare cases and only for stoichiometric HfO_2 stacks or NC up to now.[15,34] Here, it is obtained for a microchannel device based on stoichiometric, monoclinic HfO_2 NC stabilized by TOPO. Additional stable, unipolar volatile threshold switching curves recorded for 2.5 µm and 5.0 µm devices are given in Supplementary Information, Figures S10 and S11.

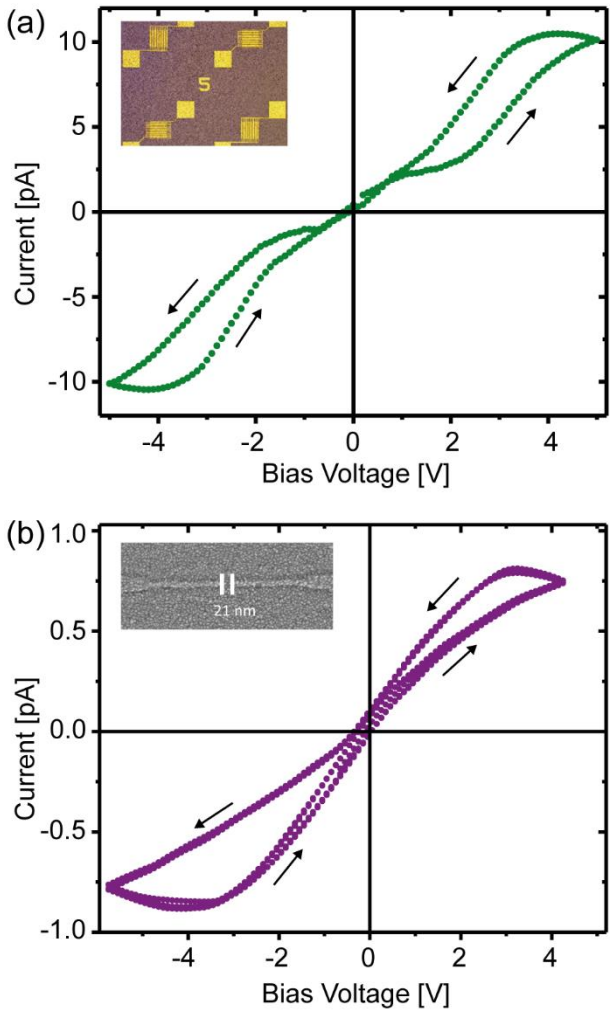

Figure 8. *I*/*U* curves of rodlike NC(dry) films recorded by periodic voltage sweeps in a (a) microelectrode device (channel width 5 µm, sweep rate of 10 mV/sec). Inset: microchannel

device. (b) Nanoelectrode device (nanoelectrode separation 21 nm, sweep rate 100 mV/sec). Inset: SEM image of a nanoelectrode device with rodlike nanoparticles.

In principle, the same hysteretic *I*/*U* characteristic is observed for nanogap devices (Figure 8b). Without any forming step they also exhibit repeatable, unipolar volatile threshold switching. However, here the increase in current, which was observed for the microchannel device at an applied voltage of 2 V, starts right at the beginning of the voltage sweep. This points to an electric field driven process starting at 2 V in the microchannel device and starting directly in the nanogap device, as an electric field of 0.4 V/µm (as applied to the microchannel device) corresponds to an applied voltage of 8 mV over a nanogap of 20 nm. In addition, slightly asymmetric unipolar hysteresis curves, like shown in Figure 8b, could be recorded. This behaviour is attributed explicitly to the device geometry of the nanogap device. A nanogap exhibiting a distance of 20 nm can be bridged by a few TOPO-HfO_2 NC and thus, makes each electrode/NC interface individual with respect to the particular distance between the electrode surface and the nearest nanocrystal resulting in a slight asymmetry of the nanodevice. In microchannel devices on the other hand, a universally averaged electrode-NC distance is valid for both electrodes making both electrode contacts symmetric.

At higher voltages, i.e. up to ±10 V, we could neither observe electroforming nor resistive switching of TOPO-HfO_2 NC in the dry state. This is in accordance with a report stating that forming of HfO_2 thin films (50 nm) embedded in Pt/HfO_2/Hf cells is not possible in vacuum and in contrary, the presence of moisture is needed to form the devices.[35] However, moisture needs to be excluded in TOPO-stabilized HfO_2 NC devices, since otherwise the conductivity will be dominated by the earlier discussed redox behaviour of NC(rm) and TOPO(rm) films (Figures 6 and 7).

The presence of interstitial cations (Hf or other cations through doping) or oxygen vacancies, $V_o^{\cdot\cdot}$, is one requirement for the formation of conductive filaments in HfO_2 materials and thus, for the enabling of resistive switching.[1,13] Here, we employ crystalline HfO_2 NC, which are not expected to have a high defect density, as insulating material between two metal electrodes

with a high work function. At these noble metal electrodes, no oxygen exchange reaction is possible leading essentially to an electron transport through the Au/TOPO-HfO_2 NC interface. For this scenario the main contribution to the current transport is based on an interface-limited, trap-assisted tunneling.[13,33] Most likely, in the NC(dry) film the surface of the monoclinic HfO_2 NC or the TOPO molecules may serve as charge carrier traps.

Besides driving the current through the Au/NC(dry)/Au device, the applied voltage will lead to a polarisation in the NC(dry) hybrid material opposed to the orientation of the applied electric field and its formation is consistent with the observed self-limited current. Dipols in the NC(dry) film might be (i) a few surplus not adsorbed TOPO molecules, (ii) dipoles created at the TOPO/metal interfaces, or (iii) NC(dry) dipoles. TOPO molecules are dipoles due to their polar $O^{\delta-}$-$P^{\delta+}$ bond and could reorientate in an electric field if their motion is not restricted by the coordinative bond to the NC surface. At the TOPO/metal interfaces charge injection from the electrodes at high voltages can lead to charged surface dipoles contributing considerably to the net polarisation. The dipole moment of ligand-stabilized NC considered as whole units is affected by the ligand environment and moreover, distinctly sensible to charge injection.[36] It is imaginable that a redistribution of surface charges or a charge injection at high electric fields will induce a dipole moment that will contribute to a net polarization. With respect to the time scale of the experiments, a polarization process involving orientation and migration of charged groups is likely in NC(dry) films, as the time span to measure the *I*/*U* hysteresis is rather in the range of minutes than in the range of seconds. If the electric field drops under a certain value, the field-induced polarization will vanish and the NC(dry) film will behave as a dielectric or poor semiconductor showing ohmic behavior. Thus, the observed volatile threshold switching behavior of monoclinic TOPO-stabilized HfO_2 NC measured under exclusion of moisture reflects the properties of the combination of the NC(dry) film with the used device design, rather than the properties of the individual NCs as such.

4. Conclusion

In conclusion, we synthesized sub-10 nm monoclinic TOPO-stabilized HfO_2 NC with a rodlike and spherical shape. By combining FT-IR, NMR spectroscopy, and XPS analysis both the adsorption of TOPO at the HfO_2 NC surface, as well as the possibility of TOPO desorption in the presence of moisture could be confirmed. The NC were assembled in dense films between microchannel devices and nanoelectrode structures with a gap of 20 nm employed for electrical characterization. Thorough cyclic *I*/*U* measurements revealed a substantial influence of traces of moisture during the clean-up of the NC or the thin film preparation on the electrical properties of the devices. While the experiments clearly show that the observed redox behavior can be attributed to the influence of moisture, we could address the TOPO-stabilized HfO_2 NC in both, microchannel and nanoelectrode devices, and identify volatile threshold switching in vacuum. The latter sweeping performance is most probably based on polarizable dipoles present in the NC(dry) film, such as surplus TOPO molecules, surface dipols at the TOPO/NC interface, or TOPO-HfO_2 NC dipoles regarded as a unit. These dipols may reorientate or their charge center may migrate under the influence of the applied electric field causing the unipolar threshold switching in the symmetric device configuration. In vacuum, reactions leading to reduced Hf or to oxygen vacancies in highly crystalline monoclinic NC are suppressed and herewith the possibility of electroforming. This detailed analysis indicates that the observed volatile threshold switching is a property of the TOPO-stabilized HfO_2 NC film in the chosen symmetric nanodevice geometry.

AUTHOR INFORMATION

Corresponding Author

*Email: s.karthaeuser@fz-juelich.de

Orcid

Sonam Maiti: 0000-0002-2217-0727.

Thorsten Ohlerth: 0000-0002-2169-8765.

Niclas Schmidt: 0000-0002-8439-8495.

Stephan Außen: 0000-0001-9083-5404.

Rainer Waser: 0000-0002-9080-8980.

Ulrich Simon: 0000-0002-6118-0573.

Silvia Karthäuser: 0000-0003-3953-6980.

Author Contributions

S.M. and T.O. contributed equally to this work.

Notes

The authors declare no competing financial interest.

SUPPORTING INFORMATION

The supporting information is available free of charge on the ACS Publications website at DOI:

Additional experimental details, SAED, XPS and *I*/*U* measurements.

ACKNOWLEDGMENTS

The authors gratefully acknowledge the assistance of Chen Liu, Grigory Potemkin, Jochen Friedrich, and Stephan Masberg. This work has been funded by Deutsche Forschungsgemeinschaft (DFG) through SFB 917 “Nanoswitches”.

References

[1] Banerjee, W.; Kashir, A.; Kamba, S. Hafnium oxide (HfO_2) – A multifunctional oxide: a review on the prospect and challenges of hafnium oxide in resistive switching and ferroelectric memories. *Small* **2022**, 2107575/1-50.

[2] Vescio, G.; López-Vidrier, J.; Leghrib, R.; Cornet, A.; Cirera, A. Flexible inkjet printed high-k HfO_2-based MIM capacitors. *J. Mater. Chem. C* **2016,** *4*, 1804-1812.

[3] Shang, J.; Xue, W.; Ji, Z.; Liu, G.; Niu, X.; Yi, X.; Pan, L.; Zhan, Q.; Xu, X.-H.; Li, R.-W. Highly flexible resistive switching memory based on amorphous-nanocrystalline hafnium oxide films. *Nanoscale* **2017,** *9*, 7037-7046.

[4] Karthäuser, S.; Peter, S.; U. Simon, U. Integration of individual functionalized gold nanoparticles into nanoelectrode configurations: Recent advances. *Eur. J. Inorg. Chem.* **2020**, 3798-3810.

[5] Mennicken, M.; Peter, S. K.; Kaulen, C.; Simon, U.; Karthäuser, S. Transport through redox-active Ru-terpyridine complexes integrated in single nanoparticle devices*. J. Phys. Chem. C* **2020**, *124*, 4881-4889.

[6] Babajani, N.; Kaulen, C.; Homberger, M.; Mennicken, M.; Waser, R.; Simon, U.; Karthäuser, S. Directed Immobilization of Janus-AuNP in Heterometallic Nanogaps: a Key Step Toward Integration of Functional Molecular Units in Nanoelectronics. *J. Phys. Chem. C.* **2014,** *118*, 27142-27149.

[7] Schmidt, D. O.; Raab, N.; Noyong, M.; Santhanam, V.; Dittmann, R.; Simon, U. Resistive switching of sub-10 nm TiO_2 nanoparticle self-assembled monolayers. *Nanomaterials* **2017**, *7*, 370.

[8] Schmidt, D. O.; Hoffmann-Eifert, S.; Zhang, H.; La Torre, C.; Besmehn, A.; Noyong, M.; Waser, R.; Simon, U. Resistive switching of individual, chemically synthesized TiO_2 nanoparticles. *Small* **2015**, *11*, 6444-6456.

[9] Dirkmann, S.; Kaiser, J.; Wenger, C.; Mussenbrock, T. Filament growth and resistive switching in hafnium oxide memristive devices. *ACS Appl. Mater. Interfaces* **2018,** *10*, 14857-14868.

[10] Petzold, S.; Zintler, A.; Eilhardt, R.; Piros, E.; Kaiser, N.; Sharath, S. U.; Vogel, T.; Major, M.; McKenna, K. P.; Molina-Luna, L.; et al. Forming-free grain boundary engineered hafnium oxide resistive random access memory devices. *Adv. Electr. Mater.* **2019,** *5*, 1900484.

[11] Dittmann, R.; Strachan, J. P. Redox-based memristive devices for new computing paradigm. *APL Mater.* **2019,** *7*, 110903.

[12] Slesazeck, S.; Mikolajick, T. Nanoscale resistive switching memory devices: a review. *Nanotechn.* **2019**, *30*, 352003/1-23.

[13] Dittmann, R.; Menzel, S.; Waser, R. Nanoionic memristive phenomena in metal oxides: the valence change mechanism. *Adv. Phys.* **2022**, *71*, 1-105.

[14] Murray, C. B.; Norris, D. J.; Bawendi, M. G. Synthesis and characterization of nearly monodisperse CdE (E = sulfur, selenium, tellurium) semiconductor nanocrystallites. *J. Amer. Chem. Soc.* **1993,** *115*, 8706-8715.

[15] Wang, J.; Choudhary, S.; De Roo, J.; De Keukeleere, K.; Van Driessche, I.; Crosby, A. J.; Nonnenmann, S. S. How ligands affect resistive switching in solution-processed HfO_2 nanoparticle assemblies. *ACS Appl. Mater. Interfaces* **2018,** *10*, 4824-4830.

[16] Tang, J.; Fabbri, J.; Robinson, R. D.; Zhu, Y.; Herman, I. P.; Steigerwald, M. L.; Brus, L. E. Solid-solution nanoparticles: Use of a nonhydrolytic sol−gel synthesis to prepare HfO_2 and $Hf_xZr_{1-x}O_2$ nanocrystals. *Chem. Mater.* **2004,** *16*, 1336-1342.

[17] Lüssem, B.; Karthäuser, S.; Haselier, H.; Waser, R. The origin of faceting of ultraflat gold films epitaxially grown on mica. *Appl. Surf. Sci*. **2005**, *249*, 197-202.

[18] Hardtdegen, A.; Zhang, H.; Hoffmann-Eifert, S. Tuning the performance of $Pt/HfO_2/Ti/Pt$ ReRAM devices obtained from plasma-enhanced atomic layer deposition for HfO_2 thin films. *ECS Trans*. **2016**, *75*, 177-184.

[19] Hilliard, C. R.; Bhuvanesh, N.; Gladysz, J. A.; Blümel, J., Synthesis, purification, and characterization of phosphine oxides and their hydrogen peroxide adducts. *Dalton Trans.* **2012,** *41*, 1742-1754.

[20] Doan-Nguyen, V. V. T.; Carroll, P. J.; Murray, C. B. Structure determination and modeling of monoclinic trioctylphosphine oxid. *Acta Cryst*. **2015**, C*71*, 239-241.

[21] Joo, J.; Yu, T.; Kim, Y. W.; Park, H. M.; Wu, F.; Zhang, J. Z.; Hyeon, T. Multigram scale synthesis and characterization of monodisperse tetragonal zirconia nanocrystals. *J. Am. Chem. Soc*. **2003**, *125*, 6553-6557.

[22] Liu, H.; Owen, J. S.; Alivisatos, A. P. Mechanistic study of precursor evolution in colloidal group II−VI semiconductor nanocrystal synthesis. *J. Am. Chem. Soc.* **2007,** *129*, 305-312.

[23] Verbelen, B.; Dahaen, W.; Binnemans, K. Selective substitution of $POCl_3$ with organometallic reagents: Synthesis of phosphinates and phosphonates. *Synthesis* **2018**, *50*, 2019-2026.

[24] De Keukeleere, K.; Coucke, S.; De Canck, E.; Van Der Voort, P.; Delpech, F.; Coppel, Y.; Hens, Z.; Van Driessche, I.; Owen, J. S.; De Roo, J. Stabilization of colloidal Ti, Zr, and Hf oxide nanocrystals by protonated tri-n-octylphosphine oxide (TOPO) and its decomposition products. *Chem. Mater.* **2017,** *29*, 10233-10242.

[25] Kahro, T.; Tarre, A.; Käämbre, T.; Piirsoo, H.-M.; Kozlova, J.; Ritslaid, P.; Kasikov, A.; Jogiaas, T.; Vinuesa, G.; Duenas, S.; et al. Hafnium oxide/graphene/hafnium

oxide-stacked nanostructures as resistive switching media. *ACS Appl. Nano Mater*. **2021**, *4*, 5152-5163.

[26] *NIST X-ray Photoelectron Spectroscopy Database*; Naumkin, A. V., Kraut-Vass, A., Gaarenstroom, S. W., Powell, C. J., Eds.; National Institute of Standards and Technology: Gaithersburg, 2012.

[27] Potts, S. E.; Dingemans, G.; Lachaud, C.; Kessels, W. M. M. Plasma-enhanced and thermal atomic layer deposition of Al_2O_3 using dimethylaluminium isopropoxide, $[Al(CH_3)_2\ (\mu\text{-}O^iPr)]_2$, as an alternative aluminium precursor. *J. Vac. Sci. Technol.* **2012**, *30*, 021505/1-12.

[28] Beamson, G., Briggs, D. *High Resolution XPS of Organic Polymers, the Scienta ESCA300 Database.* Wiley: Chichester, 1992.

[29] Morris-Cohen, A. J.; Donakowski, M. D.; Knowles, K. E.; Weiss, E. A. The effect of a common purification procedure on the chemical composition of the surfaces of CdSe quantum dots synthesized with trioctylphosphine oxide. *J. Phys. Chem C* **2010**,*114*, 897-906.

[30] Cook, A. G.; Mason, G. W. Structural effects on the acid-base properties of some closely related phosphinic acids and phosphine oxides, *J. Org. Chem.,* **1972**, *37*, 21, 3342-3345.

[31] Zheng, A.; Liu, S. B.; Deng, F. ^{31}P NMR Chemical Shifts of Phosphorus Probes as Reliable and Practical Acidity Scales for Solid and Liquid Catalysts, *Chem. Rev*., **2017**, *117*, 12475-12531.

[32] Hayashi, S. Sealing effect of magic-angle-spinning rotors in solid-state NMR. *Anal. Sci.* **2009**, *25*, 133-136.

[33] Xiao, M.; Shen, D.; Futscher, M. H.; Ehrler, B.; Musselman, K. P., Duley, W. W.; Zhou, Y. N. Threshold switching in single metal-Oxide nanobelt devices emulating an artificial nociceptor. *Adv. Electron. Mater*. **2020**, *6*, 1900595/1-12.

[34] Petzold, S.; Miranda, E.; Sharath, S. U.; Munoz-Gorriz, J.; Vogel, T.; Piros, E.; Kaiser, N.; Eilhardt, R.; Zintler, A.; Molina-Luna, L.; et al. Analysis and simulation of the multiple resistive switching modes occurring in HfO_x-based resistive random access memories using memdiodes. *J. Appl. Phys.* **2019**, *125*, 234503.

[35] Lübben, M.; Wiefels, S.; Waser, R.; Valov, I. Processes and effects of oxygen and moisture in resistively switching TaO_x and HfO_x. *Adv. Electron. Mater.* **2018**, *4*, 1700458/1-11.

[36] Nevidimov, A. V.; Razumov, V. F. The effect of stabilizing ligands on the interaction between colloidal quantum dots of cadmium selenide. Computer simulation. *Colloid J.* **2018**, *80*, 676-683.

TOC Graphic